
Bounded at both ends: the detection window of routine 12-day C-band InSAR at rock–ice avalanche sources

Measurements at Ronti Peak (Chamoli) and Langtang Lirung, with six published detections placed against it

Ajay Kumar Sah

Purbanchal University School of Engineering, Biratnagar, Nepal

ajayshah2005@gmail.com

ORCID: https://orcid.org/0009-0004-8543-4306

Companion to:

Sah, A. K. (2026) *No detectable precursor in Sentinel-1 backscatter before the 26 August 2026 Langtang Lirung rock–ice avalanche, Nepal.* EarthArXiv, doi:10.31223/X59N5N

Sah, A. K. (2026) *Calibrated detection limits in routine Sentinel-1 products 50.6 hours before the Langtang Lirung rock–ice avalanche, Nepal.* EarthArXiv, doi:10.31223/X5KZ3G

Analysis code, derived data and the verification script are archived at Zenodo, doi:10.5281/zenodo.22728130

Prepared 12 September 2026.

Keywords: Sentinel-1, InSAR coherence, detection limits, phase unwrapping, rock–ice avalanche, precursor detection, Himalaya, Chamoli, Langtang, Nepal

---

Abstract

A negative result from satellite radar — “no precursory deformation was detected” — carries no information unless the range of signals the measurement could have detected is reported alongside it. We measure that range at two rock–ice avalanche sources, Langtang Lirung, Nepal (2026) and Ronti Peak, India (2021), using a single procedure, and identify four determinants of it that are site-specific and not predictable from the sensor specification.

Viewing geometry cannot be selected on usable-pixel fraction, the quantity most easily computed before processing: at Langtang an ascending track covering 100 per cent of the source disc has **4.1 times the variance** of a descending track covering 44 per cent, and the failure is invisible on the former (z = −0.52) while the latter registers it at z = +3.65. The limiting seasonal term is variance rather than offset, and so cannot be detrended away: nine same-window February controls at Ronti span 6.95 to 32.11 per cent of the source disc below a coherence threshold, a range wider than any plausible precursor. Control design does not transfer; the published 120-disc scheme admits 46 candidates at Ronti, aspect-limited. And the upper bound is rarely stated at all. Placed against the half-fringe unwrapping limit of a 12-day pair, **no published precursory detection we examined lies inside the range a single pair can measure** — three sit at or below its floor, three at or above its ceiling, and every one was obtained by multi-epoch inversion accumulated over years rather than from the routine product.

Neither event is detectable at its source in routine 12-day C-band products, for opposite reasons: one below the precision floor, one above the unwrapping ceiling. The sensitivity range is bounded at both ends, both bounds are site-specific and differ by an order of magnitude between sites of the same hazard class, and a null reported without them is not interpretable.

---

1. Introduction

Sentinel-1 has become the default instrument for retrospective analysis of high-mountain slope failures, because it is free, global and has a consistent 12-day repeat. Published analyses report precursory deformation at several sites — a maximum line-of-sight rate of 27 mm/yr at Maoxian (Intrieri et al., 2018), a maximum of 57.3 mm/yr in the Sedongpu source area (Luo et al., 2022), and 150 mm of line-of-sight movement between June and October 2020 before the Elliot Creek failure (Geertsema et al., 2022). The first two are maxima over a source area rather than characteristic rates, and all three are line-of-sight projections; we state this because those are the conditions this paper argues must travel with any reported value.

Each is a **detection**, and all are satellite-borne. A detection establishes that a slope moved. It does not establish what a comparable measurement would have missed elsewhere, and so it cannot be inverted into a statement about monitoring capability.

Detections by other instruments are a separate class and are treated separately here: at Chamoli, ground seismometers recorded precursory signals for 2.5 hours before detachment (Tiwari et al., 2022), on the same slope where the satellite products examined below contain nothing testable.

The complementary claim — a **bound** — is rarer, because it requires the detection floor to be measured rather than assumed. Two companion papers report such bounds for the 26 August 2026 Langtang Lirung rock–ice avalanche. Sah (2026a) reports no detectable precursor in Sentinel-1 backscatter at 12-day sampling on the ascending orbit, with a measured amplitude detection limit of approximately 1 dB of progressive change over two months — against an event step of −13.3 dB, 42σ. Sah (2026b) establishes two bounds on the descending record: no surface disturbance above approximately 2 ha of coherent decorrelation in the twelve days ending 50.6 hours before failure, and no line-of-sight displacement above approximately 13 mm per month over the preceding seven weeks. The coherence statistic is calibrated against the event itself at z = +4.57 as published — +3.65 when recomputed here from raw rasters, see §6.1.

A bound at one site invites the obvious question: does the procedure transfer? The 7 February 2021 Chamoli rock–ice avalanche is the natural test. It is the same hazard class, a larger event at 26.9×10^6 m^3, on a source with better viewing geometry and three times as many usable pre-event intervals. If the procedure transfers anywhere, it should transfer there.

It does not. This paper reports why, and argues that the reasons are general enough that the sensitivity range should be reported alongside any null from these products.

---

2. Sites, data and procedure

2.1 Sites

The two sources are of the same hazard class — rock–ice avalanches initiating on glacierised high-altitude faces — and differ in almost every respect that governs a radar measurement.

Langtang Lirung, Nepal. The 26 August 2026 failure, 02:52:10 UTC (08:37:10 Nepal time). The study area spans 308 km^2, elevations 2426 to 7180 m, with only 2.12 per cent below 3000 m and all of that in the north-west corner, so the runout terminus and barrier lakes lie at the boundary rather than inside it. This is a source-area analysis and the AOI was drawn to make that explicit.

Ronti Peak, Uttarakhand, India. The 7 February 2021 Chamoli failure, 04:51 UTC, established seismically by Tiwari et al. (2022): 26.9×10^6 m^3, approximately 80 per cent bedrock, on a north-facing slope. The study area is taken from the authors' own deposited pre-event DEM (Bhushan and Shean, 2021), with processing performed on a 15 × 15 km sub-area centred on the source.

The events differ in season (monsoon against winter), in latitude, in the published motion of the source block, and — as §3 shows — in every determinant of what a routine product could have detected.

2.2 Source discs, and a coordinate that was wrong by 572 m

Both analyses use a 500 m-radius disc on the source, following the design of Sah (2026b). The Langtang disc is centred at 28.2853 N, 85.5252 E, the published value.

The Ronti disc was initially centred on the starting-zone coordinate given in the Mani et al. (2023) event database, 30.37263 N, 79.72759 E — a peer-reviewed compilation with per-event references, but a single point rather than a mapped detachment. Reading the authors' own deposited elevation-difference map (Shean et al., 2021; 2 m, EPSG:32644) shows this to be **572 m from the scar**. Within a 3 km window, 0.941 km^2 lost more than 20 m of elevation, mean loss 64.4 m and maximum 181 m, with a centroid at **30.37775 N, 79.72698 E**. The innermost 125 m of a disc on the compilation point lost no elevation at all, and only 14.6 per cent of such a disc falls on the scar.

All Ronti results below are computed on the recentred disc. The recentred disc also agrees independently with the field description: Tiwari et al. (2022) give the detached wedge as 5525 m, NNE aspect, 35° slope; the disc measures 5607 m, aspect 4.7–28.8°, slope 41.1° on Copernicus GLO-30 — elevation within 80 m and aspect consistent.

We report this because the correction is not incidental. A starting-zone coordinate from a compilation and a mapped detachment outline are different objects, and at this site they differ by more than a disc radius.

It is also the second instance of the same sensitivity within this programme. At Langtang, Sah (2026b) tested two candidate disc centres 477 m apart and found the alternative — on gentler ground, with 50 per cent more usable pixels — returned a detection bound of 22.1 per cent of the usable disc against 10.8 per cent for the disc adopted, more than twice as weak, and showed no coherence signature of the collapse at all. Disc placement at the few-hundred-metre scale is therefore not a detail of either analysis; it is a determinant of what either could have resolved.

2.3 Products, and what their stated resolution means

Three product families, identical in settings at both sites.

Viewing geometry. Copernicus Data Space Browser exports of local incidence angle, shadow mask and data mask, orthorectified on the Copernicus 30 m DEM, one export per relative orbit since these quantities are fixed per orbit. Requested at 10 m; the download dialog delivers 8.6 m, which must be stated whenever pixel counts are compared across product families.

Coherence. ASF HyP3 INSAR_GAMMA, 10 × 2 looks, DEM included, for every consecutive 12-day pair in the pre-event window.

Amplitude. GAMMA0 terrain-corrected VV and VH at 10 m. The validity mask is not static — its positive-backscatter clause moves with the data — so it must be intersected across dates within a track before differencing.

A note on posting, because it governs how the coherence results should be read. The 10 × 2 look products are posted at **40.0 m**. A 500 m disc therefore contains **489 pixels**, and all sixteen Ronti intervals return valid data across the whole disc, so intersecting validity removes none of them. Earlier reporting of this series quoted approximately 8800 disc pixels; that figure counts pixels after resampling the products onto a finer grid and is not a count of independent looks. The disc has always held about 490 of them. Two consequences follow and are used throughout: the 1500-pixel minimum in the published control design is a 10 m amplitude criterion and is not satisfiable on 40 m coherence products at any radius; and coherence rasters are thresholded at native posting, without interpolation, for the reason set out in §6.1.

Frame selection is not a formality. ASF frame numbering is not stable across years for the same relative orbit — Langtang descending relative orbit 19 is frame 497 in 2026 and frames 495 and 500 in 2019 — so relative orbit is the stable key and the frame number an along-track label. More consequentially, distance from the source to the footprint edge determines whether a product contains the source at all. Measured edge distances: Langtang frame 497, 98 km; frame 495, 10.7 km; frame 500, **3.7 km**. The frame-500 products returned empty over the source while 62 per cent valid scene-wide. At Ronti the corresponding distances are frame 492, 28.6 km; frame 488, 11.4 km; frame 493, **3.2 km**, and frame 493 was avoided on that basis. A descending swath is a rotated parallelogram whose edge is a slanted line, not a latitude, so footprint membership must be tested by point-in-polygon distance rather than by comparing corner coordinates.

Orbit direction alone is also insufficient to identify a track. Both Ronti descending tracks pass within eight minutes of each other — relative orbit 63 at approximately 00:43 UTC and relative orbit 165 at approximately 00:35 — and selecting by direction produced a misattributed geometry measurement that was caught only by checking acquisition time.

2.4 The three tests

Identical at both sites, and fixed before any result existed.

1. **Viewing geometry per relative orbit.** Median local incidence angle, layover and shadow fractions, and usable-pixel fraction under the published mask (dataMask > 0, no shadow, LIA ≤ 70) on the source disc.

2. **Coherence threshold fraction.** The percentage of usable disc pixels with coherence below 0.15, for every consecutive 12-day interval in the pre-event window, scored against the population of quiet intervals. Langtang offers five to six such intervals; Ronti offers fifteen, plus one spanning the failure.

3. **Amplitude difference across the failure.** Disc against reference terrain at 3–8 km, in both polarisations, with the Langtang case additionally scored against 120 matched control discs selected on local incidence angle, aspect and slope.

The last pre-event acquisition reaches 50.6 hours before failure at Langtang, and 196.1 hours on Ronti relative orbit 63 — the track carrying the coherence series — with relative orbit 165 reaching 28.3 hours, the tightest of any geometry examined here.

2.5 Use of AI-assisted technology

The analysis code used to produce the results and figures reported here, and the initial drafting of this manuscript, were produced with assistance from Claude (Anthropic), a large language model, in interactive sessions during September 2026. The model was used to write the processing and statistical code, to generate the figures, to check the cited literature against primary sources, and to draft text. All satellite data acquisition and export, the choice of acquisition dates and orbits, and the interpretation of results are the author's. The author has verified the reported values by running the accompanying verification script, which is archived with the derived data and recomputes every measured quantity in this paper directly from the source rasters. The author accepts full responsibility for the content.

One correction arising from that verification is reported in §6.1, together with the superseded values it replaced.

3. Four determinants of the window

3.1 Viewing geometry, and why coverage is the wrong criterion

The four source-disc geometries measured here span almost the full range the sensor offers (Figure 1). On the Langtang source, the ascending track covers **100 per cent** of the disc, has no shadow at all and a median local incidence angle of 22.6°. The descending track over the same disc has a median of 71.0°, sits partly beyond the 70° usable limit, and loses **24.6 per cent** of the disc to shadow, leaving 44.3 per cent usable. On every criterion available before processing, the ascending geometry is the better target by a wide margin.

It is also the geometry on which the event is invisible. Scored on the coherence threshold fraction, the failure-spanning interval reaches **z = +3.65** on the descending record and **z = −0.52** on the ascending one — below the ascending quiet mean, that is, inside the noise and on the wrong side of it. The reason is variance, not signal. The ascending quiet population has a standard deviation of **8.04 per cent** against **3.97** on descending: twice the scatter, **4.1 times the variance**, on the same source, the same event and the same statistic.

Foreshortening at 22.6° buys complete coverage and spends it on noise. The geometry that sees every pixel of the disc measures worse than the geometry that sees fewer than half of it.

The practical consequence is that geometry cannot be selected on usable-pixel fraction, which is the quantity most easily computed before processing. It must be selected on measured variance, which requires processing first. **This inverts the usual order of operations.**

The principle is not new here. Sah (2026b) reports it twice within the Langtang scene: applying the incidence and shadow filter to the poorer of two descending tracks deepened the post-event amplitude drop from −3.63 to −5.56 dB while reducing the sample, because near-grazing pixels sit close to the noise floor and have little room to fall; and a candidate source disc 477 m away, on gentler ground with 50 per cent more usable pixels, showed no coherence signature of the collapse at all — 13.0 per cent against a quiet mean of 12.5, against 18.0 per cent and z = +4.57 for the disc adopted. That paper states the conclusion directly: more usable pixels does not mean more detection power.

What is added here is the measurement across sites. The effect is quantified on four source geometries at two events, and the penalty is given as a number: the best-covered geometry of the four carries 4.1 times the variance of the worst-covered, and the event that one registers at z = +3.65 the other places below its own quiet mean. The principle demonstrated within one scene is shown to hold across two, and its cost is measured rather than described.

An independent instance of the same effect appears in the published record. Luo et al. (2022) discarded the ascending orbit over the Sedongpu Basin entirely, because at that site it was severely limited by layover and shadow, and worked on descending data alone. The direction that fails differs; the principle — that viewing geometry rather than coverage governs what is measurable — does not.

All four values above are computed on the raw 40 m products under the published mask. Both Langtang geometries were originally scored through the interpolation step described in §6.1, which returned 7.27 against 2.80 — a variance ratio of 6.7 rather than 4.1 — and a descending failure z of +4.57 rather than +3.65. The conclusion is unchanged and the corrected contrast remains large; the magnitude was overstated.

3.2 Season, and why the limiting term is variance rather than offset

At the Ronti source the threshold fraction roughly doubles between seasons. Within the fifteen quiet pre-event intervals, the ten spanning August to November average **11.02 ± 2.38 per cent** and the five spanning December to January average **23.60 ± 4.23 per cent**. Nine independent same-calendar-window controls drawn from February 2022 to 2026 average **19.34 ± 8.64 per cent**, which is indistinguishable from the winter population (Welch $p = 0.240$) and distinct from the autumn one ($p = 0.021$). February at this source behaves like winter.

A seasonal offset could be removed by detrending. A seasonal **variance** cannot. The nine February controls span **6.95 to 32.11 per cent** — a range wider than any plausible pre-failure signal, and wider than the total separation between the seasons it sits in. At this site, in this season, the statistic has no sensitivity left to remove a trend from.

The consequence for a null is direct. An event occurring in February must be scored against a population whose standard deviation is 8.64 percentage points. The Chamoli failure interval, at 13.50 per cent, reaches **z = −0.68** against those controls. No bound follows, and none is claimed. The limitation is not that the event was quiet; it is that the baseline is too noisy in that season to say.

Detrending was considered and declined. Fifteen points spanning a single monotone half-cycle, with the test point at the end, is a configuration in which the residual at the test point is largely determined by the choice of fit. Removing the trend would require a second season of pre-event observations, which do not exist for this event.

3.3 Control design, and its non-transferability

The design published with the Langtang coherence bound (Sah, 2026b) requires 120 control discs of the same radius as the source, at least 2 km from it, matched on local incidence angle, aspect and slope. It is the design that makes an amplitude measurement at Langtang quantitative: the interval spanning the failure gives −2.362 dB on the source disc against +0.169 ± 0.443 dB across the 120 controls, z = −5.71, and the first clean post-event interval returns z = +0.82. Both are measured in this work.

It cannot be constructed at Ronti. Across a 361 km^2 area of interest on track 63, **4,415 candidate positions pass the incidence-angle band and only 46 survive the ±35° aspect match** — against the 120 required. Enlarging the area of interest to test whether the constraint was one of extent made the result worse, because the additional terrain faces the wrong way. The binding constraint is aspect: the massif does not contain 120 slopes resembling a 41° north-facing face.

The published design is therefore not a universal procedure but a description of what Langtang's terrain happened to permit. Reporting a control-based null without stating whether the control population could be constructed is incomplete, and the failure is silent — a design that cannot be built returns no error, only a smaller number of controls and an unstated loss of power.

The cost at Ronti is specific and appears in §5: the recentred source disc brightened by +0.600 dB across the failure in both polarisations, the sign expected if bedrock replaced snow, and **we cannot say whether that is significant**, because the population needed to test it does not exist at this site. A null and an untestable positive are reported identically in the absence of controls, and they are not the same thing.

3.4 The upper bound, which is rarely stated

A detection floor is a statement about precision. An unwrapping ceiling is a statement about ambiguity, and it is the determinant most often left out. A single interferometric pair can resolve displacement unambiguously only up to half a fringe — 13.8 mm in the line of sight for Sentinel-1's 55.46 mm wavelength. Beyond that the phase wraps, and a slope moving fast enough to alias returns the same featureless result as a slope that is not moving at all. The two are indistinguishable in the reported statistic.

Our two sources sit on opposite sides of this limit.

	reported motion	per 12-day pair	vs 13.8 mm half-fringe ceiling
Langtang	10 mm/month	~3.5 mm LOS	0.25× — **below the floor**
Langtang bound (Sah, 2026b)	12.8 mm/month over 48 d	5.1 mm LOS	0.37× — the measured floor
Ronti	5–20 m/yr	164–658 mm	12–48× — **above the ceiling**

The Ronti figures are those reported by Van Wyk de Vries et al. (2022), who measure the horizontal velocity of the collapse block at 5 to 20 m/yr by optical feature tracking, with total 2016–2021 displacement of 20 to 30 m horizontally and 25 to 40 m once corrected for viewing angle. They state that at velocities of tens of metres per year the interferometric measurements are prone to phase aliasing and underestimation of the true displacement — the ceiling, reported by the authors of the only interferometric study of this source.

The published detection record sits outside the single-pair window

Placing the detections cited in §1 against the same limits is, we think, the clearest statement of the problem, because it uses other people's measurements rather than our own.

site	reported rate	per 12-day pair	vs ceiling	where
Maoxian	27 mm/yr, max LOS	0.89 mm	0.06×	below the floor
Sedongpu	57.3 mm/yr, source max LOS	1.88 mm	0.14×	below the floor
Langtang	13 mm/month, our bound	5.1 mm	0.37×	**is** the floor
Elliot Creek	150 mm, Jun–Oct 2020	14.8 mm	**1.07×**	at the ceiling
Ronti	5–20 m/yr	164–658 mm	12–48×	above the ceiling
Sedongpu glaciers, by POT	57–74 m/a	1873–2433 mm	135–176×	far above

Not one of these detections lies inside what a single 12-day C-band pair can measure. Three sit at or below the floor — Maoxian nearly six times below it, Sedongpu nearly three times, and the Langtang bound defining it — one sits essentially on the unwrapping limit, and two are above it. Every one of the interferometric detections was obtained by multi-epoch inversion accumulated over years — 45 images at Maoxian, 201 interferograms at Sedongpu, a multi-year stack on two ascending orbits at Elliot Creek — and the fastest entry is not interferometric at all.

Sedongpu appears twice, and the pair is the point: one basin, one sensor, overlapping years, measured near the floor by interferometry and three orders of magnitude above the ceiling by offset tracking, because the two methods see different surfaces.

The literature that establishes InSAR as a precursor-detection tool therefore does not establish it for the routine product, and the distinction is rarely drawn. Three caveats attach: these are maxima rather than characteristic rates; most are line-of-sight projections whose slope-parallel equivalents are larger; and the Elliot Creek figure annualises to 9.9 mm per pair, reaching the ceiling only at its summer rate. None of them moves a site across a boundary.

Detection floors are routinely reported. Unwrapping ceilings are not.

The Sedongpu Basin supplies an independent demonstration of the ceiling that does not rely on our own processing, and that we have read in full from both primaries rather than inferred. The basin has been analysed twice with Sentinel-1 over overlapping periods. Luo et al. (2022) applied SBAS-InSAR from January 2016 to October 2018 and report a maximum of 57.3 mm/yr, on coherent points concentrated on exposed rock and gravel. Li et al. (2025) applied pixel-offset tracking with SBAS from 2014 to 2022 and report maxima of 74 m/a on glacier SDP1 and 57 m/a on SDP2, with cumulative displacements exceeding 500 m and 300 m.

The factor of a thousand between them is not a disagreement. Li et al. state the reason for their method choice directly: InSAR coherence cannot be maintained on these glaciers because the motion is too rapid, so offset tracking was used instead. The two studies measure different surfaces in one basin — the slow rock that stays coherent, and the fast ice that does not — and between them they exhibit the ceiling at a single site, on a single sensor, with the method choice documented by the practitioners rather than inferred by us.

The two techniques' usable ranges are, on these parameters, nearly contiguous. Half a fringe over twelve days is 0.42 m/yr. Li et al. give their POT-SBAS precision as about one-thirtieth of a pixel, which on a 2.33 m range pixel at their 60-day baseline is 0.47 m/yr at one standard deviation. Interferometry cannot unwrap much above half a metre per year and offset tracking cannot resolve much below it. **Above the ceiling the remedy is a different technique, not a different orbit, frame or processing chain**, and where a source is known to be moving at metres per year, offset tracking is the measurement that regime admits.

A reported InSAR rate is conditional on the motion having stayed inside the unwrapping limit, and that condition is almost never stated.

---

4. The descending record at Ronti

Van Wyk de Vries et al. (2022) processed the ascending orbit at this source and set the descending record aside in a single clause, as "heavily affected by layover artifacts". No quantity is attached to that assessment, and we could locate none elsewhere in their paper.

Measured on the recentred source disc, the descending geometry does not show it. Relative orbit 63 has a median local incidence angle of **45.0°**, shadow over **0.1 per cent** of the disc, layover over 0.1 per cent, a minimum incidence angle of 16.8° and **97.1 per cent of the disc usable** under the published mask. Relative orbit 165 gives 51.3°, 1.5 per cent shadow and 91.6 per cent usable. For comparison, the Langtang descending geometry on which a bound *was* obtained runs to 71.0° with 24.6 per cent shadow and 44.3 per cent usable. **Track 63 is the best of the four source geometries measured in this study**, including both Langtang tracks.

There is also a second descending track. Relative orbit 165 is not named anywhere in their paper, and its last pre-event acquisition falls **28.3 hours** before the failure, against 196.1 hours for track 63 and 50.6 hours for the Langtang record. It is the tightest approach to a failure of any geometry examined here.

This is not a correction of an error, and we do not present it as one. Their other stated reasons hold, and they apply to the ascending track they used just as much as to the descending ones: the source is north-facing, which limits illumination; the block moved downslope toward roughly NNE while the Sentinel-1 line of sight is close to east–west, so the motion is oriented where the radar is least sensitive on *either* orbit; and at velocities of tens of metres per year the measurements are prone to phase aliasing and underestimation, which no choice of orbit repairs. Roughly half of their 108 interferograms lost coherence entirely, mostly to snow cover between November and May. Their overall conclusion — that Sentinel-1 InSAR would not have been an adequate monitoring tool at this site even with prior knowledge of where the instability lay — is one our own results support rather than contradict.

One caveat belongs with that measurement and should travel with it. It is made on a 500 m disc over the detachment. Their area of interest is larger, and a scene-wide characterisation of layover on the descending track could be accurate while the source disc itself is clean — indeed the companion paper finds exactly that asymmetry at Langtang, where two tracks differ far more over the source disc than they do scene-wide (Sah, 2026b, §3.2). We measured the disc because the disc is what a source-area analysis scores; we have not measured their scene.

The narrower point, then, is that the geometry over the source was dismissed without a measurement of the source, and the measurement does not support the stated reason there. What follows from that is not a detection. Section 3.4 makes clear why: at 5 to 20 m/yr the motion is 12 to 48 times the half-fringe ceiling, so clean geometry cannot deliver a phase measurement here regardless of which descending track is chosen. **Good geometry does not repair aliasing.** The descending record remains unexamined at this source, on better geometry than the record that was examined, and what it can support is a bound rather than a detection — one this paper does not compute, for the seasonal reason set out in §3.2.

5. Discussion

The bound literature is drawn from favourable terrain. Detections at Maoxian, Sedongpu and Elliot Creek come from vegetated, rock or deglaciating slopes in temperate or dry-season conditions. The events that generate the deadliest transboundary cascades originate on glacierised, snow-covered, high-altitude faces during monsoon or accumulation seasons — the regime in which the four determinants above are least favourable. Performance demonstrated in the first setting does not transfer to the second, and our two sites are both in the second.

At Chamoli a precursor existed and was recorded — by a different instrument. Tiwari et al. (2022) report seismic precursory signals continuously active for 2.5 hours before the main detachment, from ground stations. The failure was not unheralded. It was unheralded *in these products*. This is the cleanest available demonstration that a null from routine satellite radar is a statement about the measurement, not about the slope, and it is the reason the sensitivity range must travel with the null.

A published contrast, not a corroboration. Earlier drafts of this paper claimed that at Sedongpu deformation was measurable across the basin but *not within the avalanche source area itself*, and read that as independent support for our result. **Checking the primary shows the opposite, and the claim is withdrawn.** Luo et al. (2022) report that most coherent points in the Sedongpu Basin lay in the source area at the top of the mountain, on exposed rock and gravel; 7109 points were detected in the source branch gully, 708 of them moving faster than 20 mm/yr in line of sight, with a maximum of 57.3 mm/yr; and the spatial pattern of the deformation was highly consistent with the source area mapped by field survey. Source-area precursory motion at Sedongpu was **detected, not missed**.

What separates that result from ours is method, not site. It rests on 73 descending Sentinel-1 acquisitions from October 2014 to October 2018, 201 interferograms surviving coherence screening, SBAS inversion, 64 ground control points in stable terrain, and a spatio-temporal atmospheric filter. Most of the basin moved below 10 mm/yr and the active source points above 25 mm/yr, with a maximum of 57.3 — between three and fifteen times below the 156 mm/yr (13 mm/month) floor that a single 12-day pair supports at Langtang. Sedongpu measures what multi-epoch inversion reaches, and by contrast shows how far short of it a routine product falls. That is the same relationship set out for the two Sedongpu analyses in §3.4, and it is a contrast rather than corroboration.

It also supplies a partial answer to a question left open by the companion paper. Sah (2026b) closes by asking what precision a multi-epoch inversion over the Langtang frame would have to beat, and records that no such inversion had been published. Sedongpu shows what one delivers on a comparable target: 201 interferograms with ground control and a spatio-temporal atmospheric filter resolve source-area motion at tens of millimetres per year, roughly an order of magnitude below the 12.8 mm per month that routine twelve-day products supported at Langtang. The gap between the two is the interval in which a screening system would have to operate, and it is a gap in processing rather than in data.

One detail does transfer directly and supports §3.1. Luo et al. discarded the ascending orbit entirely, because at this site it was severely limited by layover and shadow, and worked on descending data alone. That is an independent instance of viewing geometry, not coverage, determining what is measurable — reached on a different continent for the same reason.

What a practitioner should take from this. Select geometry by relative orbit, not orbit direction, and verify by acquisition time. Check footprint edge distance before processing; at 3.7 km the product was empty over the source while 62 per cent valid scene-wide. Establish the seasonal baseline before scoring a winter event. Do not assume a control design transfers. **Never interpolate a raster before applying a fixed threshold to it —** bilinear resampling of our own coherence products biased every threshold fraction low by 1.9 to 7.4 points and compressed the variance by a fifth (§6.1), and because the bias depends on each scene's spatial structure it cannot be removed afterwards. And report the window — floor and ceiling — alongside any null.

A consequence of §3.3 worth stating explicitly. At Ronti the recentred amplitude difference is +0.600 dB on the scar, in both polarisations, of the sign expected if the detachment exposed bedrock beneath snow. We cannot say whether that is significant, because the control population required to test it does not exist at this site. The failure of the control design (§3.3) therefore does not merely weaken the analysis — **it removes the ability to evaluate a signal that is present.** A null and an untestable positive are reported identically in the absence of controls, and they are not the same thing.

What this paper does not say. It does not say InSAR is unsuitable for slope monitoring. It says routine 12-day C-band products have a measurable sensitivity range that varies by an order of magnitude between sites of the same hazard class, and that a null without that range attached cannot be interpreted.

Figures

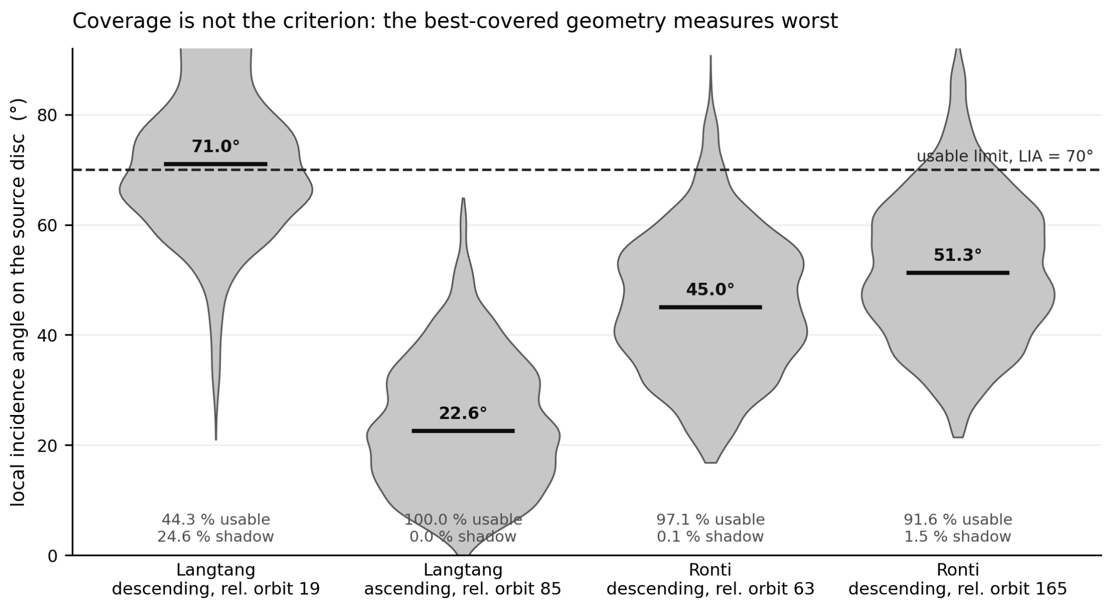

Figure 1. Local incidence angle on the four source discs. Distributions of local incidence angle within the 500 m source disc for each relative orbit examined, from Copernicus Data Space Browser geometry exports orthorectified on the Copernicus 30 m DEM. Bars mark medians; the dashed line is the LIA = 70° usable limit of the published mask. Usable and shadow fractions are annotated. The panels are ordered to make the paper's first point visible: Langtang ascending has the best coverage of the four geometries and the lowest incidence angles, and it is the geometry on which the failure is invisible (§3.1). Coverage and measurement quality are not the same quantity, and only the first can be computed before processing.

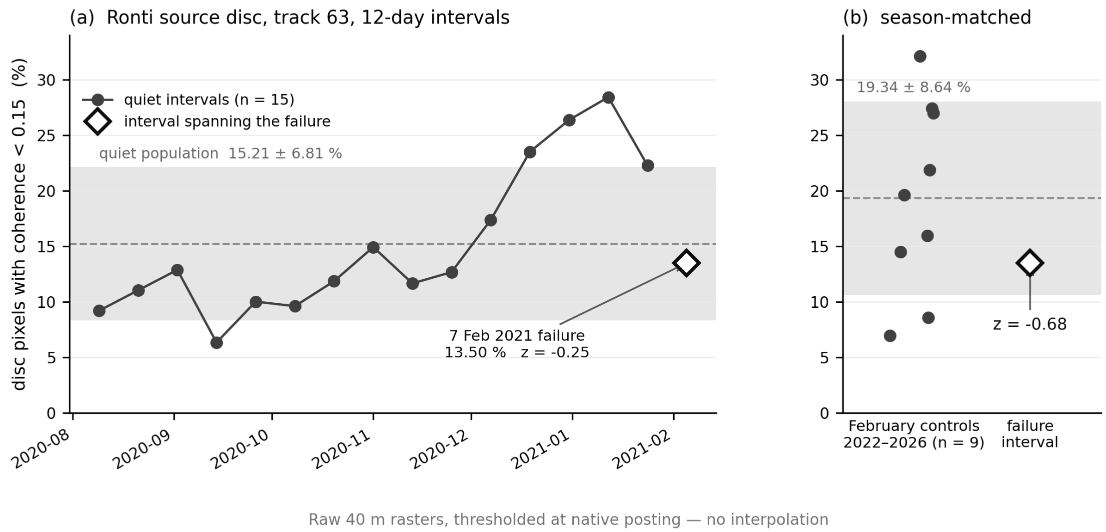

Figure 2. The coherence threshold fraction at the Ronti source, and why no bound follows from it. (a) Percentage of usable source-disc pixels with coherence below 0.15, for sixteen consecutive 12-day intervals on descending relative orbit 63, August 2020 to February 2021. The band is the quiet population mean ± one standard deviation (15.21 ± 6.81 %, n = 15); the open diamond is the interval spanning the 7 February 2021 failure, at 13.50 %, z = −0.25. (b) The same statistic for nine same-calendar-window February controls from 2022 to 2026 (19.34 ± 8.64 %), against which the failure interval scores z = −0.68.

All values are computed on the 40 m products at native posting. The series was previously reported from rasters bilinearly resampled to a finer grid before thresholding, which depressed every value and compressed the spread; see §6.1.

The monotone rise across the last five intervals of panel (a) is a seasonal signal, and it invites detrending. We have not detrended it. Fifteen points spanning a single monotone half-cycle, with the test point at the end, is a configuration in which the residual at the test point is largely determined by the choice of fit rather than by the data. Removing that trend would require a second season, not a better model — which is the same limitation recorded in §6.2, that all available controls are post-event.

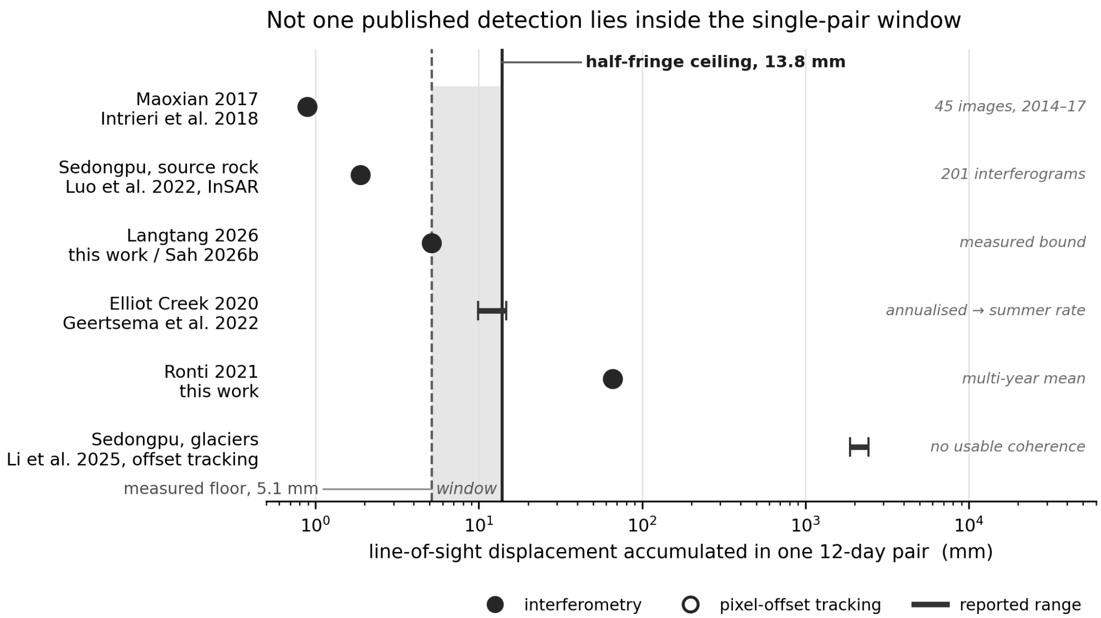

Figure 3. The sensitivity window of a single 12-day C-band pair, with the published detection record placed on it. Horizontal axis is line-of-sight displacement accumulated in one 12-day pair, logarithmic. The shaded band runs from the measured detection floor at Langtang (13 mm/month, 5.1 mm/pair) to the half-fringe unwrapping ceiling (13.8 mm/pair). Filled markers are interferometric; the open marker is pixel-offset tracking, whose own precision floor is roughly 0.47 m/yr on these parameters. The bar at Elliot Creek spans its annualised and summer rates. The right-hand column gives the acquisition burden behind each detection. Sedongpu appears twice, by two methods, in one basin.

No detection examined here lies inside the window. The three at or below the floor were resolved only by multi-epoch inversion accumulated over years; the three at or above the ceiling are aliasing-limited on a single pair. The floor plotted is the one measured at Langtang and is itself geometry-dependent by a factor of 4.1 in variance (§3.1), so it should be read as one measured instance rather than a constant.

---

6. Limitations

6.1 A correction to our own processing, and what it cost

Every coherence figure for Ronti in earlier versions of this analysis was computed on rasters that had been resampled from their native 40 m posting onto a ~9.4 m grid by **bilinear interpolation** before the 0.15 threshold was applied.

Bilinear interpolation pulls values toward the local mean. Applied before a fixed threshold, it thins whichever tail is sparser and depresses the fraction below the threshold. Re-running the identical analysis on the raw 40 m rasters reproduces the difference exactly: bilinear 11.17 ± 5.48 % against raw 15.21 ± 6.81 % on the 2020–21 series, and bilinear 14.65 ± 7.75 % against raw 19.34 ± 8.64 % on the nine February controls, the latter within

0.06 points of the value previously reported. Nearest-neighbour resampling returns the raw value; the artefact is interpolation, not resampling.

The bias is not a constant offset. It ranged from 1.93 to 7.38 points across the sixteen intervals and scaled with the quantity measured, so it compressed the sd by about a fifth. It is therefore not correctable after the fact — the affected quantities had to be recomputed, and have been.

	as previously reported	corrected
quiet mean ± sd, 2020–21	10.90 ± 5.55	**15.21 ± 6.81**
failure interval	7.70 %	**13.50 %**
z vs 15 quiet	−0.58	**−0.25**
February controls	14.71 ± 7.93	**19.34 ± 8.64**
z vs season-matched controls	−0.88	**−0.68**
Welch, controls vs Aug–Nov	0.014	**0.021**
Welch, controls vs Dec–Jan	0.267	**0.240**

No conclusion in this paper changes. The Ronti null holds, no detection is claimed, no bound was or is claimed, and February still behaves like winter rather than summer. The seasonal argument of §3.2 is *strengthened*, because the true variance is larger than the compressed figure it was originally made on.

The Langtang series carries the same artefact, and has now been recomputed. Both geometries were re-scored on raw 40 m products under the published mask:

	as reported	corrected
descending quiet ± sd	5.10 ± 2.80	**8.77 ± 3.97**
descending failure	18.00 %	**23.29 %**
descending z	+4.57	**+3.65**
ascending quiet ± sd	13.15 ± 7.27	**17.48 ± 8.04**
ascending failure	9.48 %	**13.29 %**
ascending z	−0.50	**−0.52**
variance ratio, asc : desc	6.7×	**4.1×**

Reconstructing the interpolation reproduces the reported values on both geometries, as it did at Ronti: bilinear gives 5.59 ± 2.68 and 17.31 descending, 13.39 ± 8.41 and 9.82 ascending, against reported 5.10 ± 2.80 / 18.00 and 13.15 ± 7.27 / 9.48.

The effect is geometry-dependent, which is why an earlier check missed it. Scored without the incidence-and-shadow mask, the descending z moves by only 0.04 between the two pipelines, because the shadowed pixels the mask removes are precisely where the interpolation does its compensating work. The artefact is invisible unless the mask is applied. Every conclusion survives — the Langtang detection remains decisive at z = +3.65

and the ascending null remains a null — but the descending calibration is 0.9 lower than reported, and any use of the +4.57 figure should be updated.

6.2 Remaining limitations

The most serious is that all nine seasonal controls are **post-event**. They describe the Ronti slope after the collapse, which is a different surface. Whether the same seasonal cycle held before February 2021 is untested and cannot be tested from these data. The seasonal finding should be read as establishing that the February baseline is high and erratic *at this site now*, not that it was so before the failure.

Two sites. One geometry export per track. No bound is computed at Ronti; this paper reports why one could not be.

---

7. Conclusion

Better geometry, worse result. The Ronti source offers more than twice the usable pixels of the Langtang source and three times the quiet baseline, and yields no bound, because the limiting factors are seasonal variance and unwrappable motion rather than viewing angle. Four determinants of the window — geometry, season, control design and the unwrapping ceiling — are site-specific in ways not predictable from the sensor specification, and each is measured here rather than argued.

The window they define is narrow. Between a measured floor of 5.1 mm and a half-fringe ceiling of 13.8 mm, a single 12-day pair admits less than a factor of three in displacement. Placing published precursory detections against it, none of the six examined here falls inside: three sit at or below the floor, one on the ceiling and two above it, and every interferometric detection among them was obtained by multi-epoch inversion accumulated over years rather than from the routine product. The literature establishing InSAR as a precursor-detection tool therefore does not establish it for the product most often used to report a null, and the distinction is rarely drawn.

We report a correction to our own processing on the same principle (§6.1). An interpolation step that looked like neutral reformatting biased every threshold fraction we had computed, at both sites and on all three geometries, and compressed the variance the seasonal argument rests on. No conclusion changed; every number did. The effect was also mask-dependent, and so invisible to a check that omitted the mask — which is how it survived one round of verification. That is the failure mode this paper is about, encountered from the inside.

Two consequences for practice follow. Below the floor, a null is a statement about precision and needs its floor quoted. Above the ceiling, the remedy is a different technique rather than a different orbit, frame or processing chain — as the two published analyses of the Sedongpu Basin demonstrate, one returning millimetres per year by interferometry and the other tens of metres per year by offset tracking, in the same basin on the same sensor.

A null reported without its window is not interpretable.

Data and code availability

Sentinel-1 products are freely available from the Copernicus Data Space Ecosystem and the Alaska Satellite Facility. Analysis code, derived data, the figure scripts and the verification script are archived at Zenodo, doi:10.5281/zenodo.22728130 (version 3.0.0); version 1.0.0 of that record, doi:10.5281/zenodo.22541072, holds the material for the companion backscatter study, and version 2.0.0, doi:10.5281/zenodo.22676918, that for the companion detection-limits study.

The archived package includes `verify_paper3.py`, which recomputes every measured quantity reported here directly from the source rasters and reports each against the published value. The acquisition list, evalscript and export settings needed to regenerate the input products from the free archives are given in the package README; the Sentinel-1 products themselves are not redistributed.

The elevation-difference map used to locate the Chamoli source is Shean et al. (2021), doi:10.5281/zenodo.4558692, and the pre-event digital elevation model is Bhushan and Shean (2021), doi:10.5281/zenodo.4554647. Both are freely available.

Contains modified Copernicus Sentinel data 2020–2026.

Acknowledgements

This work uses modified Copernicus Sentinel data 2020–2026, processed to orthorectified terrain-corrected products by Sentinel Hub and by the Alaska Satellite Facility HyP3 service. Elevation data are Copernicus GLO-30. The author thanks the authors of the datasets cited in Section 2 for depositing their mapped products openly; the recentring described in Section 2.2 was possible only because the Chamoli difference map is public.

The author declares no competing interests and received no funding for this work.

Use of AI-assisted technology in preparing this work is disclosed in Section 2.5, in accordance with the ICMJE recommendation that AI use in analysis and figure generation be reported in the methods.

References

Bhushan, S. and Shean, D. (2021). *Chamoli Disaster Pre-event 2-m DEM Composite: September 2015* [Dataset]. Zenodo. https://doi.org/10.5281/zenodo.4554647

Geertsema, M., Menounos, B., Bullard, G. et al. (2022). The 28 November 2020 landslide, tsunami, and outburst flood — a hazard cascade associated with rapid deglaciation at Elliot Creek, British Columbia, Canada. *Geophysical Research Letters*, 49(6). https://doi.org/10.1029/2021GL096716

Intrieri, E., Raspini, F., Fumagalli, A., Lu, P., Del Conte, S., Farina, P., Allievi, J., Ferretti, A. and Casagli, N. (2018). The Maoxian landslide as seen from space: detecting precursors of failure with Sentinel-1 data. *Landslides*, 15, 123–133. https://doi.org/10.1007/s10346-017-0915-7

Li, H., Yang, Y., Dong, X., Xu, Q., Li, P., Zhao, J., Chen, Q. and Hu, J.-C. (2025). Frequent glacial hazard deformation detection based on POT-SBAS InSAR in the Sedongpu Basin in the Himalayan region. *Remote Sensing*, 17(2), 319. https://doi.org/10.3390/rs17020319

Luo, S., Xiong, J., Liu, S., Hu, K., Cheng, W., Liu, J., He, Y., Sun, H., Cui, X. and Wang, X. (2022). New insights into ice avalanche-induced debris flows in southeastern Tibet using SAR technology. *Remote Sensing*, 14(11), 2603. https://doi.org/10.3390/rs14112603

Mani, P., Allen, S., Evans, S. G., Kargel, J. S., Mergili, M., Petrakov, D. and Stoffel, M. (2023). Geomorphic process chains in high-mountain regions — a review and classification approach for natural hazards. *Reviews of Geophysics*, 61(4), e2022RG000791. https://doi.org/10.1029/2022RG000791

Sah, A. K. (2026a). No detectable precursor in Sentinel-1 backscatter before the 26 August 2026 Langtang Lirung rock–ice avalanche, Nepal. EarthArXiv. https://doi.org/10.31223/X59N5N

Sah, A. K. (2026b). Calibrated detection limits in routine Sentinel-1 products 50.6 hours before the Langtang Lirung rock–ice avalanche, Nepal. EarthArXiv. https://doi.org/10.31223/X5KZ3G

Shean, D., Bhushan, S., Berthier, E., Deschamps-Berger, C., Gascoin, S. and Knuth, F. (2021). *Chamoli Disaster Post-event 2-m DEM Composite (February 10–11, 2021) and Difference Map* [Dataset]. Zenodo. https://doi.org/10.5281/zenodo.4558692

Shugar, D. H., Jacquemart, M., Shean, D. et al. (2021). A massive rock and ice avalanche caused the 2021 disaster at Chamoli, Indian Himalaya. *Science*, 373, 300–306. https://doi.org/10.1126/science.abh4455

Tiwari, A., Sain, K., Kumar, A., Tiwari, J., Paul, A., Kumar, N., Haldar, C., Kumar, S. and Pandey, C. P. (2022). Potential seismic precursors and surficial dynamics of a deadly Himalayan disaster: an early warning approach. *Scientific Reports*, 12, 3733. https://doi.org/10.1038/s41598-022-07491-y

Van Wyk de Vries, M., Bhushan, S., Jacquemart, M. et al. (2022). Pre-collapse motion of the February 2021 Chamoli rock–ice avalanche, Indian Himalaya. *Natural Hazards and Earth System Sciences*, 22, 3309–3327. https://doi.org/10.5194/nhess-22-3309-2022

Author lists marked "et al." are truncated at three; full author lists for every entry are recorded in `derived/references_verified_paper3.md` *in the archived package, each verified against Crossref or DataCite on 12 September 2026.*